Extreme Mechanics Letters 9 (2016) 195–203

Contents lists available at ScienceDirect

Extreme Mechanics Letters

journal homepage: www.elsevier.com/locate/eml

Giant continuously-tunable actuation of a dielectric elastomer ring actuator

Ying Shi Teh [a], Soo Jin Adrian Koh [a,b,*]

[a] Engineering Science Programme, National University of Singapore, 9 Engineering Drive 1, Kent Ridge, Singapore 117575, Singapore

[b] Department of Mechanical Engineering, National University of Singapore, 9 Engineering Drive 1, Kent Ridge, Singapore 117575, Singapore

ARTICLE INFO

Article history:
Received 11 April 2016
Received in revised form 11 July 2016
Accepted 12 July 2016
Available online 16 July 2016

ABSTRACT

Electric stimulus triggers mechanical deformation in an electroactive polymer actuator, much like the human muscle. Here, we demonstrate a dielectric elastomer actuator in a ring configuration, exhibiting electrically-induced linear strains in excess of 200%. We use theory to inspire the possibility of giant voltage-induced actuation, and create an experimental prototype of a ring dielectric elastomer actuator with continuously-tunable actuation of up to 200% strain. We further demonstrate giant actuation of a free-standing module of ring actuator, pre-tensioned using buckled carbon fibre strips, exhibiting electrically-induced mechanical linear strains in excess of 100% that is continuously-tunable with voltage. Unlike areal strains, displacements from electrically-induced linear strains may be fully utilized to do work, thereby allowing ring actuators to be integrated as actuator modules in robotic systems.

1. Introduction

A dielectric elastomer (DE) consists of a stretchable polymer membrane sandwiched between compliant electrodes. When a potential difference (ϕ) is applied on the electrodes, the resulting electric field polarizes the dielectric (polymer) and induces Maxwell stress, thereby thinning the membrane and expanding its area (Fig. 1). This phenomenon may take place in the absence of mechanical forces P_1, P_2.

Dielectric elastomer actuators (DEAs) are capable of generating high actuation strain and energy density comparable to biological muscles [1]. Hence, they are also termed "artificial muscles" [1]. Along with other attributes such as light weight, silent operation, fast response and low cost, DEAs have become a topic of great interest in the field of soft robotics [2–6], and have been studied for use as adaptive optics [7,8], refreshable Braille displays [9–11], and Sepia displays [12].

Under a moderately high electric field, DEAs undergo electromechanical instability (EMI). EMI is the positive feedback between a thinning dielectric and an increasing electric field, initiating a runaway electric field within the dielectric, leading to electrical breakdown. In the absence of pre-stretch, EMI limits voltage-induced actuation of DEAs to linear strains of between 30% and 50% [13]. In order to enhance actuation strain, one may choose to either harness EMI or eliminate it. EMI may be harnessed by carefully controlling the mechanical loading and voltage, so that the DEA will settle at an alternative stable state after experiencing EMI [14,15]. A large areal strain of 1600% has been attained using this approach, but here the DEA only operates in two bi-stable states of small and large strains. EMI may be suppressed or eliminated by pre-stretch, allowing linear or areal strains to exceed that of an unstretched DEA [16–19]. Pelrine et al. first

* Corresponding author at: Department of Mechanical Engineering, National University of Singapore, 9 Engineering Drive 1, Kent Ridge, Singapore 117575, Singapore.
E-mail address: adrian_koh@nus.edu.sg (S.J.A. Koh).

http://dx.doi.org/10.1016/j.eml.2016.07.002
2352-4316/

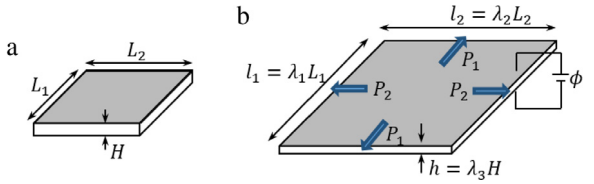

Fig. 1. Schematic of flat DE in (a) reference state and (b) stretched and charged state.

demonstrated a 158% voltage-induced area expansion of a circular acrylic elastomer membrane radially pre-stretched and attached to a rigid frame [16]. In the same study, they also demonstrated a 215% linear strain for an unequally pre-stretched membrane. This lays the basis for an unequally (orthotropically) pre-stretched DEA to achieve very high linear strains. An areal strain of 488%, which corresponds to a linear strain of 142%, was later shown using equal-biaxial dead load [18]. Following Pelrine et al.'s demonstration [16], theory was used to predict the possibility of linear strains in excess of 1000% for an orthotropically pre-stretched DEA [20, yet to be published].

Giant actuation with a record high linear strain of 500% has been demonstrated for a flat laterally-clamped DEA [21, yet to be published]. Such an actuation was made possible when the DE is pre-stretched orthotropically in one direction, while allowing deformation in the other two unconstrained Cartesian directions. Such a configuration is commonly known as "pure shear" (Fig. 2). Unlike the case with only two bistable states, here the actuation may be continuously tunable with a voltage. A flat DEA is however less durable and difficult to be incorporated into actuator systems. Rolling up the DEA into a ring configuration helps to mitigate these issues and is therefore the key focus of this paper. In the section that follows, we shall establish equilibrium equations for a generically-deformed dielectric elastomer (Fig. 1), followed by analyses for the orthotropically pre-stretched, clamped configuration and ring configuration.

2. Analysis of an orthotropically pre-stretched dielectric elastomer

Subjected to forces P_1, P_2 and a voltage ϕ, a DE membrane changes its dimensions from L_1, L_2 and H in its reference state, to l_1, l_2 and h in its stretched and charged state. As shown in Fig. 1, we quantify deformation by stretches: λ_1, λ_2 and λ_3. In our analyses, we assume that the elastomer is incompressible, giving: $\lambda_1\lambda_2\lambda_3 = 1$.

We further assume that the DE deforms under an isothermal condition. The Helmholtz free energy (Π) of the thermodynamic system therefore comprises the dielectric elastomer, the mechanical force and the electrical voltage in the actuated state, given as:

$$\Pi = L_1 L_2 H W(\lambda_1, \lambda_2, D) - P_1 l_1 - P_2 l_2 - \phi Q \tag{1}$$

$(P_1 l_1 + P_2 l_2)$ gives the mechanical work done by the elastomer, ϕQ is the electrical work done by the electric field, and the magnitude of the charge is $Q = D l_1 l_2$ with D being the electric displacement. $W(\lambda_1, \lambda_2, D)$ is the free energy density of the DE, which is the arithmetic sum of the free energy due to mechanical stretching $W_s(\lambda_1, \lambda_2)$, and the free energy due to dielectric polarization $W_p(D)$. We use the Gent hyperelastic material model to represent $W_s(\lambda_1, \lambda_2)$ [22]. An elastomer comprises of a three-dimensional network of long and highly coiled polymer chains, which are very flexible when being stretched initially but stiffens steeply when approaching the fully-stretched state [23]. The Gent model takes into account this strain-hardening behaviour as the DE approaches its stretch limit. The second term $W_p(D)$ represents the dielectric energy. Here it is assumed that the DE is a linear, ideal elastomer which polarizes almost as freely as polymer melt [23] and hence, $W_p(D) = D^2/2\varepsilon$. In this case, the electric displacement D is related to the true electric field E as: $D = \varepsilon E$. Here, we assume that the dielectric permittivity ε is independent of the state of deformation. The Gent model is given in Eq. (2), where J_{lim} is a constant related to the stretch limit and μ is the small strain shear modulus. We assume $J_{lim} = 120$, a typical value measured for acrylic-based elastomers [24].

$$W_s(\lambda_1, \lambda_2) = -\frac{\mu}{2} J_{lim} \ln\left(1 - \frac{\lambda_1^2 + \lambda_2^2 + \lambda_1^{-2}\lambda_2^{-2} - 3}{J_{lim}}\right). \tag{2}$$

We consider a DEA with orthotropic pre-stretch—stretch applied in the lateral direction and then clamped to preserve it, as shown in Fig. 2. This results in a membrane that is stretch-stiffened in one direction, while remaining compliant in the other. Previous studies have shown that DEAs utilizing such a mode of pre-stretch is able to achieve electrically-induced strains of more than 100% [21,25]. Since orthotropic pre-stretch allows the membrane to be stretch-stiffened in one direction, while allowing free actuation in the direction perpendicular to the pre-stretch, it may potentially be harnessed to do significant mechanical work induced by electrical actuation. While previous studies have demonstrated large electrically-induced strains, they have not explored if such strains induced may be further enhanced. We shall, in this paragraph, analyse this configuration to inspire the possibility of very large electrical actuation, beyond what was demonstrated previously.

In an orthotropically pre-stretched membrane, the DEA is pre-stretched in the lateral direction before it is clamped (Fig. 2(a)). In our analysis, for simplicity, we idealize that the lateral pre-stretch is preserved for the entire height of the elastomer. In reality, one may expect some relaxation of pre-stretch away from the clamps, but we shall reserve this analysis to a later section. The lateral pre-stretch is denoted by λ_{2p}. Before application of voltage, the DEA may also be pre-stretched in the longitudinal direction, for example, in the form of a fixed mechanical load P (Fig. 2(a)). We denote the stretch due to P, in the absence of voltage, as λ_{1p} (Fig. 2(a)). Under an electric field, the DEA actuates in the longitudinal λ_1 direction (Fig. 2(b)). From (1), we write the Helmholtz free energy of an orthotropically pre-stretched DEA as follows:

$$\Pi = L_1 L_2 H W\left(\lambda_1, \lambda_{2p}, D\right) - P L_1 \lambda_1 - P_2 L_2 \lambda_{2p} - \phi D L_1 L_2 \lambda_1 \lambda_{2p}. \tag{3}$$

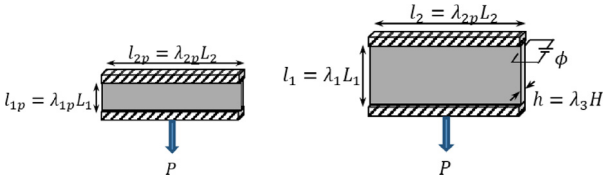

(a) Uncharged. (b) Actuated.

Fig. 2. Schematic of an orthotropically pre-stretched, laterally-clamped DEA in (a) uncharged but pre-stretched state, and (b) actuated state.

Applying the variational principle, equilibrium at any prescribed voltage ϕ is obtained when (3) is minimized by setting $\delta\Pi$ to be zero. Considering small and independent variations of extensive variables λ_1 and D, the equation-of-state for the actuator expanding in the longitudinal direction may be obtained, as follows:

$$\frac{1}{\mu}\frac{\partial W\left(\lambda_1, \lambda_{2p}, D\right)}{\partial \lambda_1} = \frac{P}{\mu L_2 H} + \frac{\varepsilon}{\mu}\left(\frac{\phi}{H}\right)^2 \lambda_1 \lambda_{2p}^2 \tag{4}$$

Eq. (4) is a statement of equilibrium—the externally-applied mechanical load (P) and the electrical stress caused by the electric field is balanced by the internal stress given by the left-hand-side. One may prescribe the external mechanical load P and the voltage ϕ, so that Eq. (4) becomes an equation with only one unknown λ_1. Solving for this unknown gives the equilibrium steady-state deformation of the DE that is laterally-constrained with a pre-stretch of λ_{2p}, subject to a combination of external loads P and ϕ.

Although a voltage on the DEA expands it in the longitudinal direction, it simultaneously relaxes the lateral stress in DE membrane due to the clamps. This relaxation with increasing voltage may be analytically captured by the nominal lateral stress quantity $P_2/(\mu L_1 H)$ in Eq. (5) below. It follows that, when the applied voltage is sufficiently large, the lateral stress will be fully relaxed. The voltage that fully relaxes the DE may be computed by setting $P_2 = 0$ in (5). From this point forward, any increase in the voltage will produce wrinkles in the membrane due to continual lateral expansion of the DE. We model this by removing the fixed lateral stretch λ_{2p} in both (4) and (5), and allowing the lateral stretch λ_2 to increase at zero lateral stress, by setting $P_2 = 0$ in (5). This is reminiscent of a DE expanding in a uniaxial fashion [19].

$$\frac{P_2}{\mu L_1 H} = \frac{1}{\mu}\frac{\partial W\left(\lambda_1, \lambda_2, D\right)}{\partial \lambda_2}\bigg|_{\lambda_2 = \lambda_{2p}} - \frac{\varepsilon}{\mu}\left(\frac{\phi}{H}\right)^2 \lambda_1^2 \lambda_{2p} \tag{5}$$

Eq. (6) gives the specialized equations for a wrinkled uniaxial actuation mode for the DEA. Since both ϕ and P are prescribed, this is a system of two unknowns (longitudinal stretch λ_1 and lateral stretch λ_2):

$$\frac{1}{\mu}\frac{\partial W(\lambda_1, \lambda_2, D)}{\partial \lambda_1} = \frac{P}{\mu L_2 H} + \frac{\varepsilon}{\mu}\left(\frac{\phi}{H}\right)^2 \lambda_1 \lambda_2^2 \tag{6a}$$

$$\frac{1}{\mu}\frac{\partial W(\lambda_1, \lambda_2, D)}{\partial \lambda_2} = \frac{\varepsilon}{\mu}\left(\frac{\phi}{H}\right)^2 \lambda_1^2 \lambda_2. \tag{6b}$$

We use Eqs. (4)–(6) to plot the voltage–stretch response of a laterally-clamped DEA. At low voltages, Eq. (4) governs

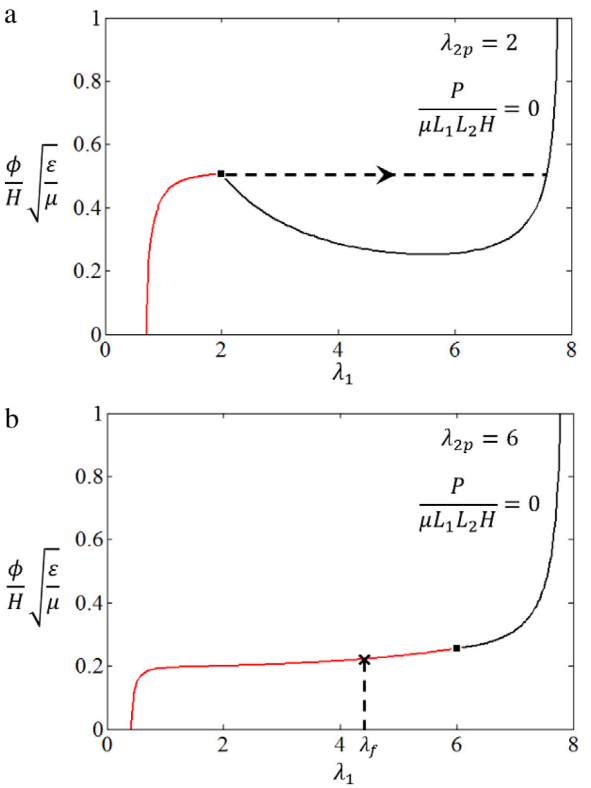

Fig. 3. Voltage–stretch response for an orthotropically pre-stretched DEA. The DEA transits from a flat, laterally-clamped mode (—— , left of square marker) to a uniaxial mode (–-, right of square marker) for: (a) $\lambda_{2p} = 2$; (b) $\lambda_{2p} = 6$. (For interpretation of the references to colour in this figure legend, the reader is referred to the web version of this article.)

and the DEA undergoes actuation in a laterally-clamped, unwrinkled state. At a critical voltage, the lateral stress fully relaxes and the DEA continues to actuate in a wrinkled uniaxial mode with increasing voltage. The critical voltage is given by (5), and further actuation in the wrinkled state is modelled by (6). We represent the laterally-clamped actuation by a red line, and the wrinkled uniaxial actuation by a black line, as shown in Fig. 3. The point of transition is denoted by a solid square. One may then expect a diverse range of actuation responses, due to different combinations of pre-stretches applied (λ_{1p} and λ_{2p}) [20]. Fig. 3 plots the case where $P = 0$, for two levels of lateral pre-stretches: $\lambda_{2p} = 2.0$ and 6.0. Fig. 3(b) inspires the possibility of very large voltage-induced actuation due to the effect of lateral pre-stretch suppressing instability, as denoted by the localized peak (solid square) in Fig. 3(a).

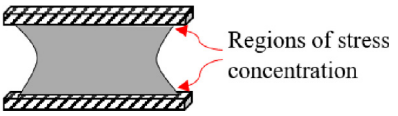

Fig. 4. Schematic showing the reality of relaxation of pre-stretch in an orthotropically pre-stretched, laterally-clamped DEA.

Fig. 3(a) shows that, at low levels of λ_{2p}, the DE undergoes electromechanical instability (EMI) at a voltage level that coincides with full relaxation of lateral stress. Any further increase in voltage would cause the elastomer to follow the dashed line, 'jumping' to a state of very large stretch and drastically thinning down the membrane. The elastomer is unlikely to survive this sudden increase in electric field, which is in the vicinity of above 500 MV/m [26]. In this mode, the DEA undergoes a modest actuation of only up to the critical voltage for full lateral stress relaxation. Fig. 3(b) denotes a suppression of instability due to large lateral pre-stretch. There are two reasons for the suppression of instability. First, a large lateral pre-stretch thins down the DEA before any voltage is applied. Hence, the same voltage applied on this DEA induces a larger electric field as compared to the case in Fig. 3(a). This induces a correspondingly larger actuation for the same voltage. Second, the larger lateral pre-stretch delays the onset of lateral stress loss. The combination of small voltage inducing large actuation and the delay of lateral stress loss moderates the net electric field on the DE, and effectively eliminates the onset of instability. This allows the DEA to undergo very large actuation before electrical breakdown terminates the process. From our analysis, we show that the utilization of a large lateral pre-stretch inspires the possibility of extremely large actuation, that is continuously-tunable by an increasing voltage. One may perform a quick calculation, by assuming a breakdown field of 200 MV/m, that electrically-induced actuation is in the excess of 1000% strain for the DEA shown in Fig. 3(b), which is indeed much larger than the case with equal-biaxial prestress shown in [19]. Here, electrically-induced actuation strain is defined as $\epsilon_{act} = \left(\lambda_f/\lambda_{1p} - 1\right) \times 100\%$, where λ_f corresponds to the stretch by which the electrical field is equal to 200 MV/m, indicated by a cross on Fig. 3(b).

An orthotropically pre-stretched and laterally-clamped DEA, as shown in Fig. 2, though exhibits an extremely large actuation, may be too bulky to be integrated into actuator systems. Furthermore, any pre-stretch will only be preserved only at the clamped edges. Away from the clamped edges, the membrane will tend to relax, reducing the pre-stretch at location away from the clamped edges (Fig. 4). Such stress relaxation away from the clamps tends to concentrate stress at the corner edges of the clamps, as indicated on Fig. 4. This leads to a significant compromise in terms of durability against repeated actuation cycles (Fig. 4). We therefore propose rolling the flat DEA membrane into a ring. The small curvature and shallow depth of the ring allows the DEA to preserve the characteristics of an approximately laterally-clamped flat membrane, while the circular geometry eliminates sharp corners, thereby removing large stress concentrators. Ring DEAs may also be readily modularized or incorporated into actuator systems. We will analyse a ring DEA, as a guide for us to design a ring actuator capable of giant, continuously-tunable actuation.

3. Analysis of a ring dielectric elastomer actuator

Following Lu et al. [24], we write a numerical model for the ring DEA, as shown in Fig. 5, with the Helmholtz free energy given as:

$$\Pi = 2\pi BH \int_{-L/2}^{L/2} W\left(\lambda_1, \lambda_2, D\right) dZ - Pl - \phi Q. \tag{7}$$

Minimizing this free energy yields the following equations-of-state:

$$\frac{d}{dZ}\left(s_1 \sin\theta\right) = 0 \tag{8a}$$

$$\frac{d}{dZ}\left(s_1 \cos\theta\right) - \frac{s_2}{B} = 0 \tag{8b}$$

$$\frac{\partial W\left(\lambda_1, \lambda_2, D\right)}{\partial D} = E \tag{8c}$$

where Z is a coordinate along the height of the ring DEA in the unloaded and uncharged state, and θ is the angle of

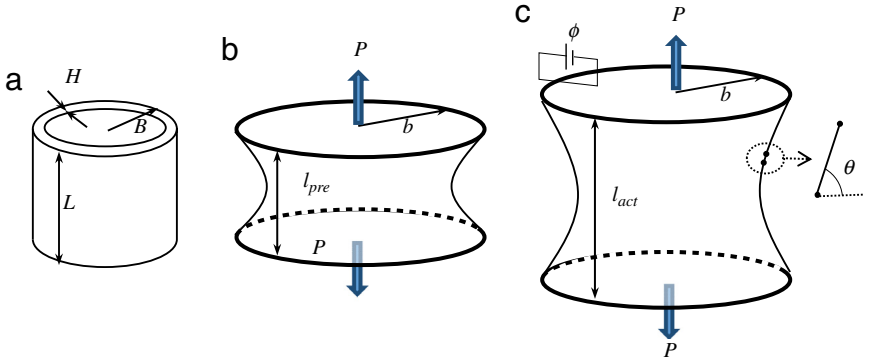

Fig. 5. Schematic of ring dielectric elastomer (DE). (a) At the unloaded and uncharged state. The DE has length L, radius B, and thickness H. (b) At the pre-stretched and mechanically-loaded state. The DE is pre-stretched in the hoop direction, and then constrained around its top and bottom circumferences by two rigid rings of radius b each. The DE is then loaded in the longitudinal direction by a dead load P, the longitudinal length becomes l_{pre}. (c) At the actuated state. Voltage ϕ is applied on the DEA, the DEA lengthens in the longitudinal direction to l, and simultaneously relaxes in stress in the hoop direction.

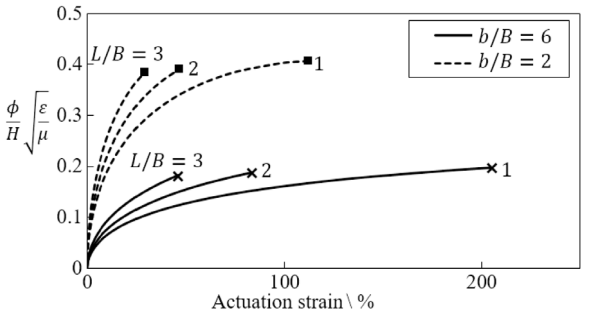

Fig. 6. Variation of actuation strain with voltage at $P/(2\pi\mu BH) = 1$. The cross mark corresponds to the point where electrical breakdown occurs, and the solid square indicates the onset of lateral stress loss at the clamped edges, which simultaneously terminates the actuation due to electromechanical instability. Maximum actuation strain ϵ_{act} is found to decrease with aspect ratio L/B but increase with hoop pre-stretch b/B.

the wall from the radial axis. s_1 and s_2 are nominal stresses. They are related to the true stresses σ_1 and σ_2 respectively and can be expressed as:

$$s_1 = \frac{\sigma_1}{\lambda_1} = \frac{\partial W(\lambda_1, \lambda_2, D)}{\partial \lambda_1} - \frac{\phi}{H} D\lambda_2 \tag{9a}$$

$$s_2 = \frac{\sigma_2}{\lambda_2} = \frac{\partial W(\lambda_1, \lambda_2, D)}{\partial \lambda_2} - \frac{\phi}{H} D\lambda_1. \tag{9b}$$

Eqs. (8) and (9) give a boundary value problem which can be solved numerically using the shooting method [24]. The predicted deformed structure of the ring DEA when subjected to a voltage can be obtained from the numerical model. A common measure of actuation performance is actuation strain as follows:

$$\epsilon = (l/l_{pre} - 1) \times 100\%. \tag{10}$$

In our preceding analysis, we assume a flat configuration with lateral pre-stretch fully preserved along the height of the DEA. In this analysis, we use a short, wide ring. Such a configuration gives a very small curvature, so that the deformation characteristics do not deviate significantly from a laterally-clamped flat DEA of zero curvature. However, unlike the preceding analysis, we analyse this system so that the hoop pre-stretch away from the clamps stress-relaxes. We model this retraction due to stress relaxation using Eqs. (7) and (8). Physically, we expect the degree of hoop retraction farthest away from the clamps to be dependent on the aspect ratio L/B (Fig. 5(a)). If L/B is very small, hoop retraction will be limited. In the limiting case of $L/B \to 0$, no retraction is possible; the DEA deforms like an ideal orthotropically pre-stretched and laterally-clamped mode if curvature $\to 0$. On the other extreme, if $L/B \to \infty$, the DEA deforms like a tube actuator in the absence of hoop pre-stretch. In reality, deformation of the DEA straddles between these two limits, depending upon L/B. As was illustrated previously, the lateral pre-stretch λ_{2p} affects the actuation response. In this example of a ring actuator, λ_{2p} manifests itself as the hoop pre-stretch b/B (Fig. 5(a), (b)). Lastly, the load $P/(2\pi\mu BH)$ causing a longitudinal pre-stretch in the absence of voltage (Fig. 5(b), (c)) is also expected to modify actuation response. We study the effects of L/B, $P/(2\pi\mu BH)$, with two levels of b/B on the actuation

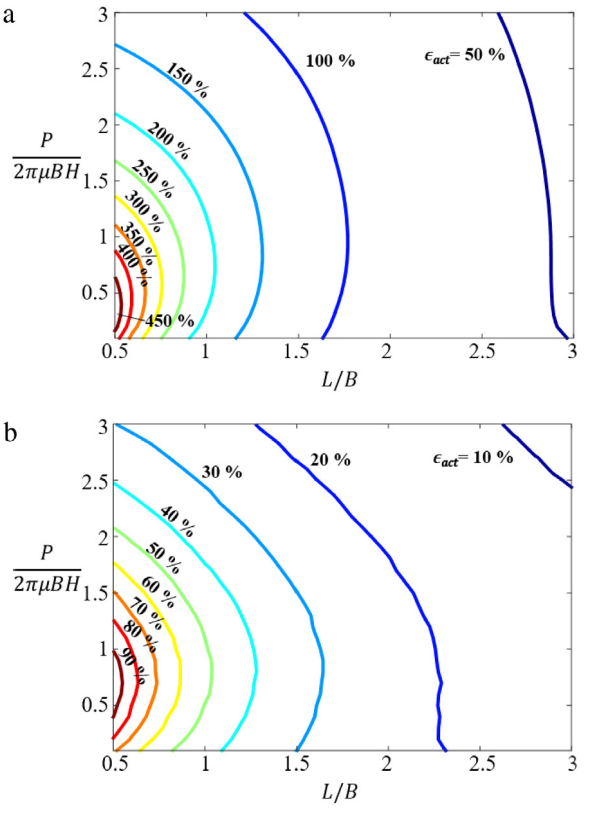

Fig. 7. Variation of maximum actuation strain ϵ_{act} with load $P/2\pi\mu BH$ and aspect ratio L/B, for (a) acrylic VHB materials and (b) natural rubber. We use hoop pre-stretch $b/B = 6$, $E_B\sqrt{\varepsilon/\mu} = 5.95$, $J_{lim} = 120$ in (a), and $b/B = 4$, $E_B\sqrt{\varepsilon/\mu} = 2$, $J_{lim} = 50$ in (b). Here ϵ_{act} refers to the strain before electrical breakdown occurs. There is no loss of tension due to the large hoop pre-stretch applied.

response of a ring DEA. To provide an indication of the maximum possible actuation, we set $E_B\sqrt{\varepsilon/\mu} = 5.95$, where E_B is the dielectric strength, ε is the dielectric permittivity and μ is the small-strain shear modulus given in Eq. (2). This value of 5.95 is representative of the commonly-used acrylic-based VHB elastomer [17,24,26,27], which material we shall use in our experiments.

At a large hoop pre-stretch b/B of 6, an applied voltage on the ring DEA relaxes its lateral or hoop stress and expands it longitudinally up till the cross mark in Fig. 6 which indicates electrical breakdown. In contrast, a DEA with a small b/B of 2 experiences total loss of hoop stress, leading to electromechanical instability and breakdown. Hoop stress or s_2 at the clamped edges of the DEA reduces to zero at the point denoted by a solid square in Fig. 6. The solid square in Fig. 6 for b/B of 2 hence corresponds to the maximum possible actuation.

Fig. 6 shows that actuation strain decreases with aspect ratio L/B, but is enhanced by hoop pre-stretch b/B. Fig. 7(a) shows there is an optimal load P for a given aspect ratio that maximizes actuation strain. We shall use $b/B = 6$, $L/B \approx 1$ with Fig. 7(a) as a guide to determine the optimized $P/2\pi\mu BH$ for our experiment.

So far we have applied the analysis to acrylic-based VHB elastomers. To predict the actuation performance of

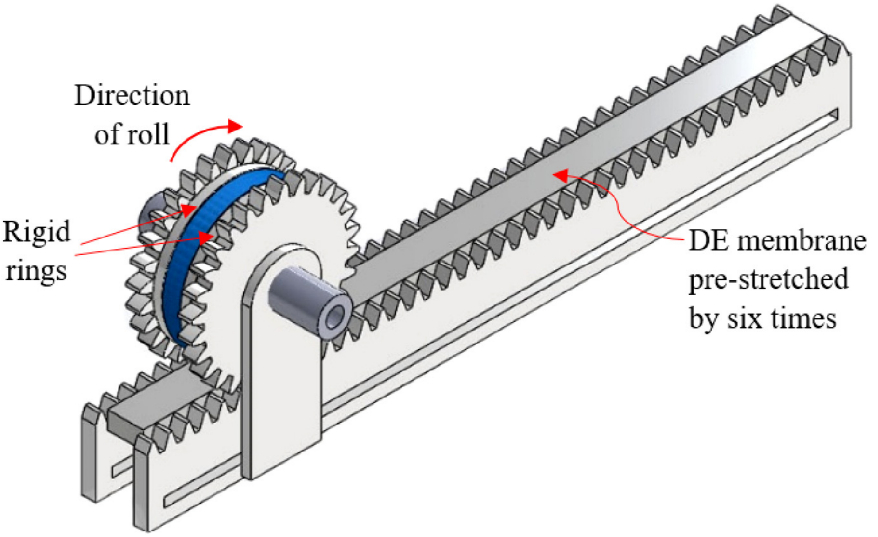

Fig. 8. A drawing of the rack-and-pinion system used to roll up a pre-stretched DE membrane onto two rigid rings.

other types of dielectric elastomers, we have to repeat the procedure using the appropriate material constants. For instance, in the case of natural rubber where $E_B\sqrt{\varepsilon/\mu} = 2$ and $J_{lim} = 50$, a hoop pre-stretch b/B of around 4 is needed to fully suppress EMI [20]. The variation of maximum actuation strain with load and aspect ratio is plotted on Fig. 7(b). Looking at $L/B = 1$ on Fig. 7(b), we obtain the maximum actuation strain to be around 50% at $P/2\pi\mu BH = 0.7$.

4. Dielectric elastomer ring actuator with large, continuously-tunable actuation

We fabricate a ring DEA using the 3M^{TM} VHB 4905 elastomer. We first pre-stretch a flat membrane by six times, and then rolling it up onto two rigid rings of 10 cm in diameter each using a rack-and-pinion system (Fig. 8). We then hang a dead load P, before applying carbon grease (Nye Nyogel 756G) as compliant electrodes. A Glassman FX60R5 high voltage power supply was used to charge the DEA. Voltage was ramped at a constant rate of 6.65 V/s and the entire actuation process was filmed. The corresponding actuation strain was computed from the image analysis of video frames. We select an aspect ratio L/B of 1.32, for the reason that this is the smallest possible aspect ratio that may be properly fabricated by the manual rack-and-pinion method. It is possible for an even smaller aspect ratio to be created with precision manufacturing of the ring DEA.

The magnitude of dead load P_{dead} affects the total actuation strain, as suggested by Fig. 7. The addition of P introduces longitudinal stretch. This longitudinal stretch tends to re-stress the stress-relaxed regions away from the clamped edges. Re-stressing of the membrane aids in the suppression of electromechanical instability, thereby enhancing the actuation strain (Fig. 9). However, as P further increased, l_{act} will saturate to the limiting stretch of the elastomer (Fig. 9), thereby limiting the total electrically-actuated stretch or strain. Based on this

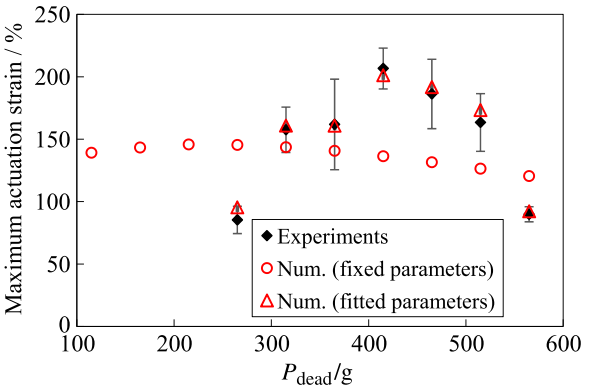

Fig. 9. Variation of maximum actuation strain with preload P_{dead} for a ring DEA with aspect ratio of 1.32. (For interpretation of the references to colour in this figure legend, the reader is referred to the web version of this article.)

observation, an optimal load that maximizes actuation exists. This qualitative observation was confirmed by the theoretical analysis as shown above (Fig. 7). The optimal load that maximizes total actuation for our experiment was observed to be around 415 g (Fig. 9). Fig. 10 shows a ring DEA fabricated using this optimal load, which gives a record high actuation linear strain of 218% before the membrane fails by electrical breakdown [28].

We plot the load-dependent electromechanical actuation limits of the DEA, by showing the initial and the maximum actuated lengths, l_{pre} and l_{act} on the same plot in Fig. 11, for various levels of P. This plot shall be used as a design plot in a subsequent section. The error bars in Figs. 9 and 11 could largely be attributed to the highly statistical nature of the elastomer itself. The lack of very precise machinery in fabricating the DEAs could also partly contribute to the errors.

We further compare our experimental results with the theoretical predictions obtained from Fig. 7, which are superimposed onto Fig. 9 as red hollow circles. While

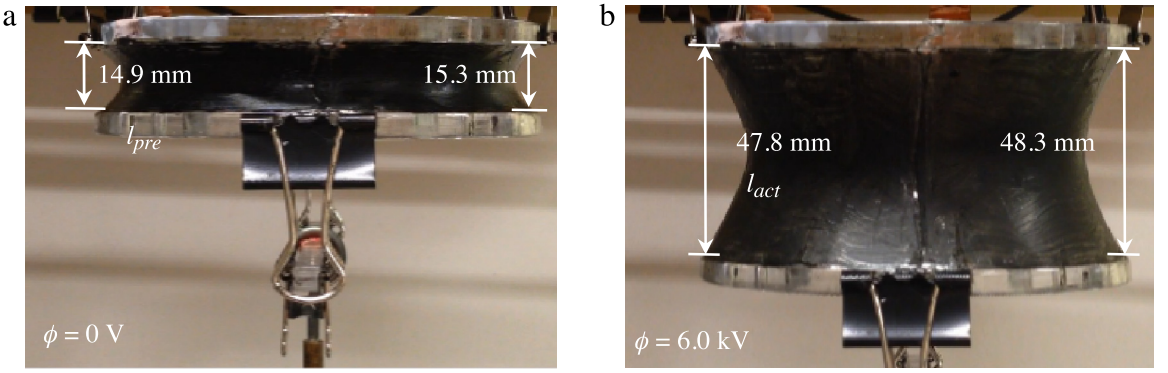

Fig. 10. Ring DEA (a) at zero voltage, and (b) at an applied voltage of 6.0 kV. (a) and (b) are of the same magnification. Comparing them gives an average actuation strain of 218% for this figure.

the results from analysis indicate the presence of an optimal load, the experimental data and the theoretical analysis display poor agreement. We attribute this to the highly statistical nature of material properties of dielectric elastomers reported in various literature, which may also be modified by the state of deformation or the level of electrical field [17,26,29–31].

To check that the actual "observed" experimental material parameters lie within the range of magnitude determined by other experiments, we produce a best fit of our theoretical model to our experiment. Fig. 12 shows an example of how analytical fitting was done for dead load of 415 g. We first obtain the variation of stretch l/L with voltage for the experiments performed. We then gradually vary the three material constants so that the analytical material parameters produce a best fit to the experimental data. This process is repeated for seven experimental data points of varying dead load, with the fitted parameters contained in Table 1. We use the analytically-fitted material parameters to compute the maximum actuation strain, and displayed them as red hollow triangles on Fig. 9.

We note that the fitted material parameters on Table 1 agree with the published values for acrylic-based VHB membranes [17,26,29–31].

5. Free-standing DEA module pre-strained with buckled carbon fibre strips

We demonstrate in the previous section, that appropriate preload optimizes the longitudinal actuation of a ring DEA (Figs. 7, 9 and 11). However, adding a dead load introduces an additional component to be integrated to an actuator system, thereby increasing the overall weight of the actuator system, and reducing its capability to be easily integrated into robotic systems. Here, we introduce the possibility of constructing a free-standing ring DEA, using buckled carbon fibre strips to pre-tension the actuator, as shown in Fig. 13. The buckled fibre strips are made of 55% unidirectional carbon fibre in resin. The buckled fibre strips introduces both longitudinal pretension and facilitates mechanical extension, allowing the actuator to perform more efficiently.

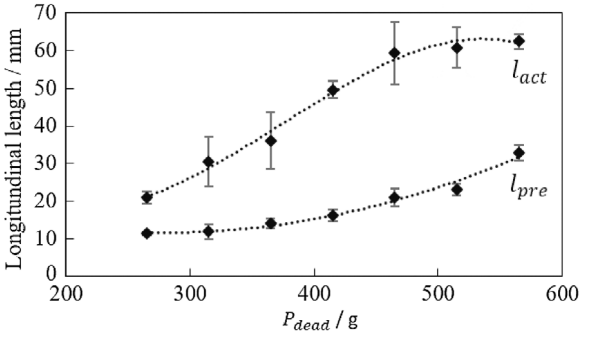

Fig. 11. Experimental variation of initial and final longitudinal lengths of a ring DEA (l_{pre} and l_{act}) with preload P_{dead}, using aspect ratio of 1.32. l_{act} denotes the maximum actuation length of the DEA before electrical breakdown occurs. The dotted lines denote trendlines for the experimental data. l_{act} approaches a limit at large P_{dead}, while l_{pre} continues to increase with preloading.

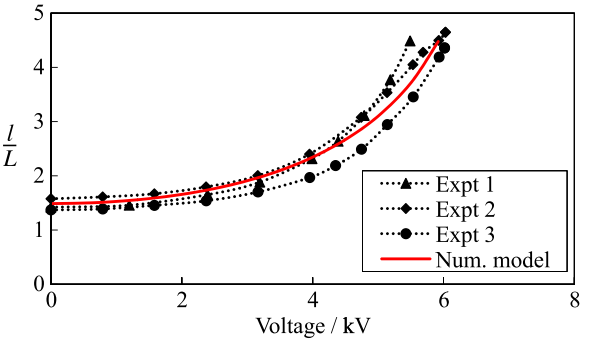

Fig. 12. Graphs of stretch against voltage used to fit the numerical model to the experimental data for P_{dead} of 415 g.

We experimentally compress a carbon fibre strip to observe how it buckles under an external axial force, and its subsequent post-buckling response. Fig. 14 shows the force–deflection response curve of a carbon fibre strip with doubly-pinned ends. The strip first follows a Hookean force–deflection response before it buckles. Beyond the buckling load F_c, it transits into a post-buckling deformation. The post-buckling behaviour of the carbon strip is affected by its length, width and thickness.

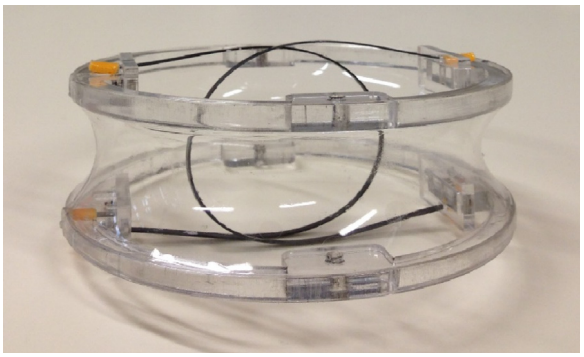

Fig. 13. DEA pre-tensioned with buckled carbon fibre strips.

Table 1
List of material constants (relative dielectric constant ε_r, shear modulus μ, and dielectric strength E_B) corresponding to different loads P_{dead} that are used as input to the numerical model for Fig. 9.

P_{dead} (g)	$\varepsilon_r = \varepsilon/\varepsilon_0$	μ (kPa)	E_B (MV m^{-1})
265	5.2	39	140
315	5.8	41	180
365	6.1	42	180
415	5.9	39	200
465	6.7	36	190
515	6.9	34	190
565	5.7	25	165

We select appropriate dimensions of the carbon fibre strips to enable large actuation of the DEA, with the aid of Fig. 11. For the ring DEA of 10 cm diameter, with $L/B = 1.32$, as presented in the previous section, the carbon strip incorporated has to be sufficiently long to provide a deflection range of at least 60 mm. We select a carbon strip of thickness 0.5 mm and effective length of 160 mm, and then size a suitable width that maximizes actuation using Fig. 15.

The blue lines on Fig. 15 were reproduced directly from Fig. 11; they show the initial and maximum attainable lengths (l_{pre} and l_{act}) of the DEA when subjected to electromechanical actuation under varying external dead weights. This serves as the equivalent force that the carbon strips impart on the actuator. We superimpose the force–deflection curves for carbon fibre strips of different widths on Fig. 15 (details of experiments on different strip widths are contained in the Supplementary Information). For a carbon strip with fixed width, for example 2.5 mm, the carbon strips apply an initial longitudinal force on the DEA, indicated by I. As voltage increases, the force in the strips relaxes, and travels along the path IF, ending at F, which corresponds to the maximum actuated length. The total actuation strain may then be computed by the total displacement traversed by the actuator between I and F, divided by its original length at I. We may then select the width that optimizes the actuation strain. From Fig. 15, the width of 2.0 mm gives the highest approximate actuation strain of 105%. We select this width to be used in our experiments, which will be presented in the next section. Obviously, this may not be the maximum possible actuation achievable for DEAs in this

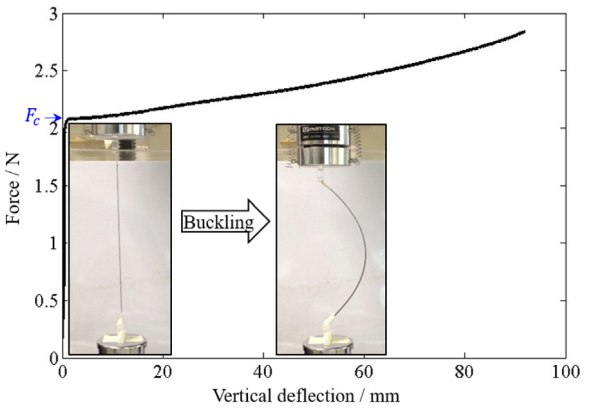

Fig. 14. A typical axial force–vertical deflection response curve of a carbon fibre strip with pinned ends, for a carbon strip of thickness 0.5 mm and effective length of 160 mm.

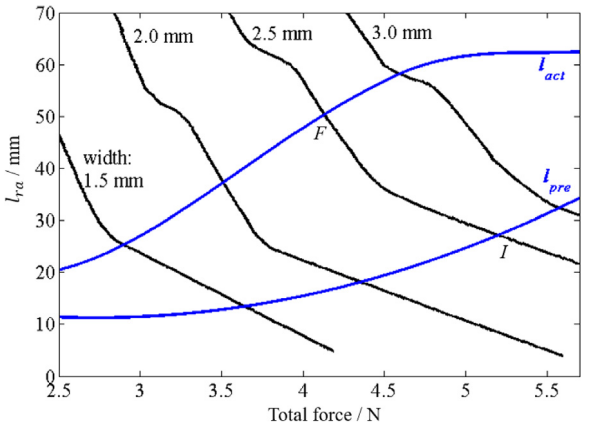

Fig. 15. Selection of a suitable width for carbon fibre strip. Blue lines denote l_{pre} or l_{act} of the DEA under varying external dead loads. Black lines denote the variation of the longitudinal lengths of the two carbon strips with force. A correction of 6 mm is employed to account for the difference in the actual actuator setup. The intersection point gives an estimate on l_{pre} or l_{act} when carbon strips of the specified width are incorporated. (For interpretation of the references to colour in this figure legend, the reader is referred to the web version of this article.)

configuration. One may immediately observe that an extremely flexible post-buckling response will further maximize the actuation strain. Detailed analyses are required to seek the maximum, which we will not do here. Instead, we shall focus on the demonstration of the possibility of very large, continuously-tunable actuation in excess of 100%, for a free-standing ring actuator using carbon strips, which has not been previously demonstrated.

We fabricate a ring DEA using two buckled carbon fibre strips of thickness 0.5 mm, effective length of 160 mm and width 2.0 mm (as suggested by Fig. 15). Fig. 16 shows the evolution of actuation strain with applied voltage for the DEA which, in the absence of EMI, is continuously-tunable with increasing voltage. In our experiment, the DEA has an initial average longitudinal length of 21.5 mm. At maximum actuation, its length is 52.1 mm, at a maximum voltage of 5.60 kV. We compute the maximum continuously-tunable actuation strain to be 142%.

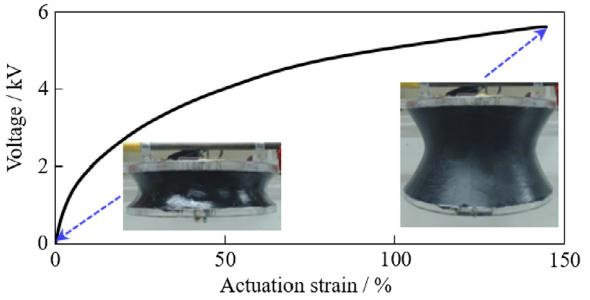

Fig. 16. Voltage–actuation strain curve of a DEA with buckled carbon fibre strips terminating at the onset of EMI.

Our design is similar in-principle to a previously proposed Tube-Spring-Actuator (TSA) [32]. A TSA uses a pre-compressed spring in-place of carbon strips to provide pre-strain. In a previous work, an axial strain of up to 25% has been shown experimentally in a TSA with VHB as the elastomer [32], limited by the amount of total pre-compression in the spring. The advantage of using buckled carbon fibre strips is that the resistance force due to the carbon strips continually reduces as the actuation increases, over a very large displacement. Conversely, the spring force reduces from a pre-compressed state to a zero force state, over a much lesser displacement. Any subsequent actuation in a TSA would increase the spring tension force, imposing restrain on the DEA from further actuation. Hence, DEAs pre-tensioned by carbon strips allows the DEA to attain much higher actuation strain as compared to a TSA. The carbon strips may be easily tuned by varying their dimensions to give the desired actuation performance.

6. Concluding remarks

Inspired by theory, we design a DEA of ring configuration that demonstrates very large continuously-tunable actuation of over 100% actuation strain. Our analyses allowed us to identify parameters and conditions for suppression of electromechanical instability and thereby optimizing actuation performance in terms of maximum electrically-induced strain. Using an optimal combination of operating conditions, we demonstrated large actuation with actuation strain of more than 200% using a preloaded ring DEA. We further demonstrated large continuously-tunable actuation for a free-standing ring DEA pre-strained with buckled carbon fibre strips, of up to 142% actuation strain. These findings will aid in the development of high performance soft actuators modules, with very large electrically-induced actuation strains that are continuously-tunable by voltage.

Acknowledgements

This work was funded by the Singapore Ministry of Education Tier 1 Grant, Faculty Research Fund, through funding code: R-265-000-500-112. Ying Shi Teh would further like to acknowledge financial support from the National University of Singapore through the Engineering Science Programme Final Year Research Project (ESP OOE acct: C533.000.003.001).

Appendix A. Supplementary data

Supplementary material related to this article can be found online at http://dx.doi.org/10.1016/j.eml.2016.07.002.

References

[1] S. Ashley, Artificial muscle, Sci. Am. 289 (2003) 52–59.
[2] P. Brochu, Q. Pei, Advances in dielectric elastomers for actuators and artificial muscles, Macromol. Rapid Commun. 31 (2010) 10–36.
[3] G. Kovacs, P. Lochmatter, M. Wissler, An arm wrestling robot driven by dielectric elastomer actuators, Smart Mater. Struct. 16 (2007) S306–S317.
[4] R. Pelrine, et al. Dielectric elastomer artificial muscle actuators: toward biomimetic motion, in: Proc. SPIE 4695, EAPAD, 2002, p. 126.
[5] S. Shian, K. Bertoldi, D.R. Clarke, Dielectric elastomer based "grippers" for soft robotics, Adv. Mater. 27 (2015) 6814–6819.
[6] J. Shintake, et al., Versatile soft grippers with intrinsic electroadhesion based on multifunctional polymer actuators, Adv. Mater. 28 (2016) 231–238.
[7] F. Carpi, et al., Bioinspired tunable lens with muscle-like electroactive elastomers, Adv. Funct. Mater. 21 (2011) 4152–4158.
[8] S. Shian, R.M. Diebold, D.R. Clarke, Tunable lenses using transparent dielectric elastomer actuators, Opt. Soc. Amer. 21 (2013) 8669–8676.
[9] P. Chakraborti, et al., A compact dielectric elastomer tubular actuator for refreshable Braille displays, Sens. Actuators A: Phys. 179 (2012) 151–157.
[10] Z. Yu, et al., Large-strain, rigid-to-rigid deformation of bistable electroactive polymers, Appl. Phys. Lett. 95 (2009) 192904.
[11] Z. Ren, et al. A new bistable electroactive polymer for prolonged cycle lifetime of refreshable Braille displays, in: Proc. SPIE 9056, EAPAD, 2014, p. 905621.
[12] S. Shian, D.R. Clarke, R.M. Diebold, Display pixel using liquid ink and elastomers, 2013.
[13] R.E. Pelrine, R.D. Kornbluh, J.P. Joseph, Electrostriction of polymer dielectrics with compliant electrodes as a means of actuation, Sens. Actuators A: Phys. 64 (1998) 77–85.
[14] C. Keplinger, et al., Harnessing snap-through instability in soft dielectrics to achieve giant voltage-triggered deformation, Soft Matter 8 (2012) 285–288.
[15] T. Li, et al., Giant voltage-induced deformation in dielectric elastomers near the verge of snap-through instability, J. Mech. Phys. Solids 61 (2013) 611–628.
[16] R. Pelrine, et al., High-speed electrically actuated elastomers with strain greater than 100%, Science 287 (2000) 836–839.
[17] T. Lu, et al., Dielectric elastomer actuators under equal-biaxial forces, uniaxial forces, and uniaxial constraint of stiff fibers, Soft Matter 8 (2012) 6167.
[18] J. Huang, et al., Giant, voltage-actuated deformation of a dielectric elastomer under dead load, Appl. Phys. Lett. 100 (2012) 041911.
[19] S.J.A. Koh, et al., Mechanisms of large actuation strain in dielectric elastomers, J. Polym. Sci., Part B: Polym. Phys. 49 (2011) 504–515.
[20] S.J.A. Koh, et al. High-performance electromechanical transduction using laterally-constrained dielectric elastomers Part I: Actuation processes. (Unpublished).
[21] Y.F. Goh, et al. Ultra-actuation of acrylic-based artificial muscles. (Unpublished).
[22] A.N. Gent, A new constitutive relation for rubber, Rubber Chem. Technol. 69 (1966) 59–61.
[23] Z. Suo, Theory of dielectric elastomers, Acta Mech. Sin. 23 (2010) 449–578.
[24] T. Lu, et al., Highly deformable actuators made of dielectric elastomers clamped by rigid rings, J. Appl. Phys. 115 (2014) 184105.
[25] J. Zhu, et al., Two types of transitions to wrinkles in dielectric elastomers, Soft Matter 8 (2012) 8840.
[26] J. Huang, et al., The thickness and stretch dependence of the electrical breakdown strength of an acrylic dielectric elastomer, Appl. Phys. Lett. 101 (2012) 122905.
[27] Y. Bar-Cohen, et al. The dielectric constant of 3M VHB: a parameter in dispute, 7287, EAPAD, 2009.
[28] Y.S. Teh, Y.F. Goh, S.J.A. Koh, Large actuation of an acrylic-based dielectric elastomer actuator in tubular configuration, in: ICEIC, 2015.
[29] G. Kofod, et al., Actuation response of polyacrylate dielectric elastomers, J. Intell. Mater. Syst. Struct. 14 (2003) 787–793.
[30] S.J.A. Koh, et al., Dielectric elastomer generators: How much energy can be converted? IEEE/ASME Trans. Mechatronics 16 (2011) 33–41.
[31] R. Kaltseis, Natural rubber for sustainable high-power electrical energy generation, RSC Adv. 4 (2014) 27905–27913.
[32] N.H. Chuc, et al., Artificial muscle actuator based on the synthetic elastomer, Int. J. Control Autom. 6 (2008) 894–903.